Spectroscopic and nanoscopic characterisation of copper metalloproteins at nanoscale for bioelectronic devices"

(Activities of the Viterbo INFM group within SAMBA, EC - FET project)

1. Self-assembling and Conductivity of Plastocyanin mutants.

INFM Viterbo group within the SAMBA project has focused its attention on the design, spectroscopic analysis and single molecule characterisation of copper protein plastocyanin mutants. The aim was to get some insight on the electron transport mechanism at molecular level, which is a fundamental task in building up hydrid nanodevices, and to implement the use of different metalloproteins (Fig.1) for interconnecting nanostructures.

The Viterbo group has closely collaborated with the Leiden group in the design and engineering of two plastocyanin mutants able to selectively bind to gold surface, by exploiting either SS or SH groups. In the first mutant (PCSS), a disulfide bridge was inserted within the protein (Fig. 1a) by replacing residues Ile-21 and Glu-25 with Cys using structurally conservative mutagenesis. X-ray crystallography and several spectroscopies (Resonance Raman, Electron Paramagnetic Resonance, UV-VIS) indicated that the overall three-dimensional structure of PCSS and the redox copper site coordination has been essentially preserved together with its electron transfer properties **(ref. 1, 5)**.

In the second mutant (PCSH) a residue tail (threonine, cysteine and glycine) at the C-terminal end was inserted (Fig. 1b). The single surface exposed thiol group should provide a further possibility for plastocyanin immobilisation. The spectroscopic characterisation of this mutant pointed out that, even in this case, the copper site coordination has been preserved **(ref. 7)**.

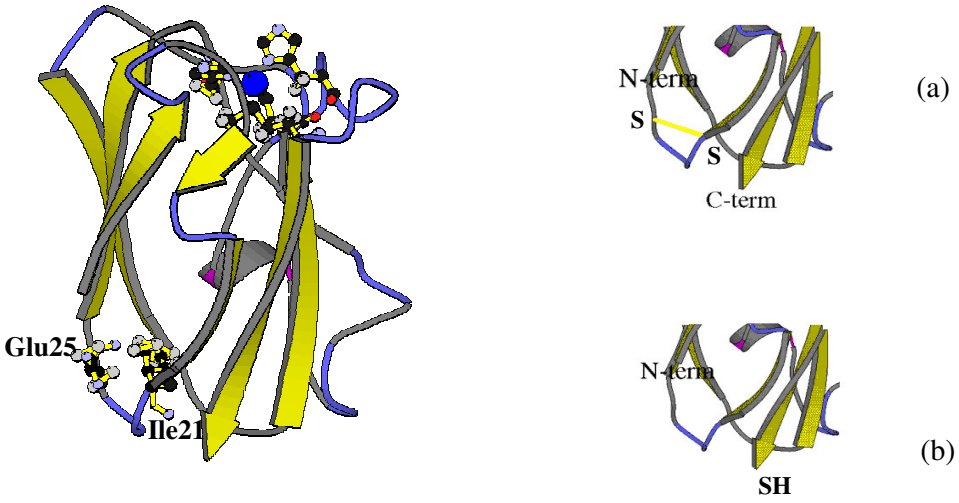

Fig. 1: The three dimensional structure of poplar plastocyanin showing the copper atom at the top surrounded by the four ligands. The amino acid residues selected for the site-directed mutagenesis and the copper ligands are labeled.

The self-assembling and the conductive properties of plastocyanin immobilised on gold surface via either SH or SS groups, were studied by using Scanning Probe Microscopy (STM/STS, Tapping Mode AFM, Conductive AFM), cyclic voltammetry (CV) and Molecular Dynamic Simulations (MDS).

Morphology of single plastocyanin mutants adsorbed on Au(111)

The morphology of adsorbed PCSS and PCSH, in particular the height and orientation of the macromolecules respect to the gold substrate was examined by a systematic analysis by TMAFM and STM **(refs. 5, 7)**.

Fig. 2 shows representative TMAFM images of PCSS (a) and PCSH (b) molecules adsorbed onto Au (111), recorded in buffer solution. Both mutants are homogeneously distributed over the substrate, whereas the high quality of the recorded image, even after repetitive scans, is indicative of a stable binding to gold. Individual molecules are well distinguishable above the substrate, and the vertical dimension of the PC mutants was estimated from individual cross section statistical analysis, as shown in Fig. 2. Data taken for hundreds of molecules are represented in the histograms of Fig. 3.

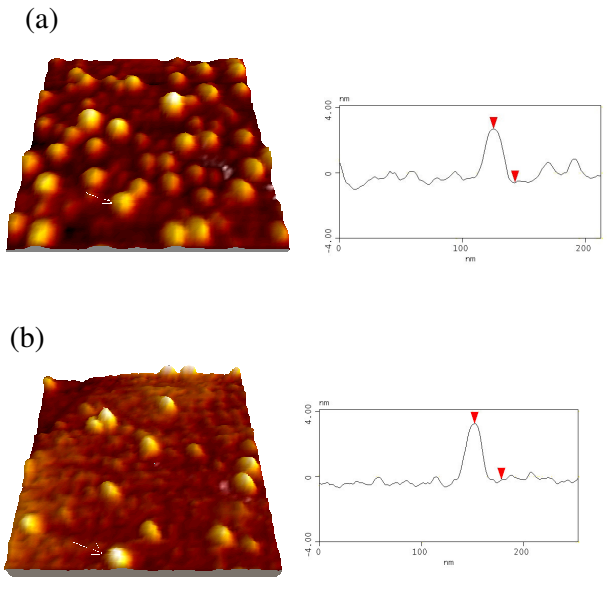

Fig. 2: TMAFM image and representative cross section profile of PCSS (a) and PCSH (b) molecules adsorbed on Au(111).

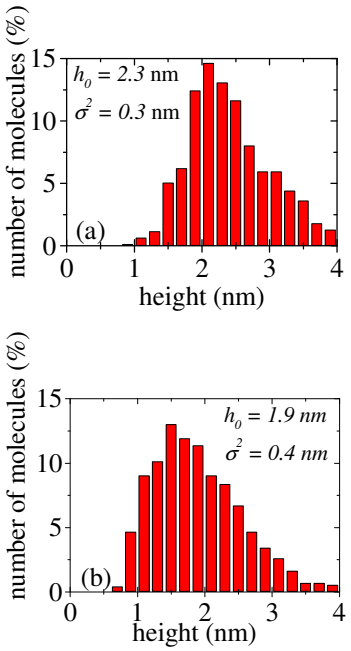

Fig. 3: Statistical analysis of PCSS (a) and PCSH (b) height above the Au(111) substrate.

The monomodal distribution is indicative of a preferential orientation of the adsorbed proteins on the gold substrate. The data for PCSS molecules have a mean value equal to 2.3 nm and a standard deviation of 0.5 nm, whereas for PCSH the mean height is 1.9 nm with a standard deviation of 0.6 nm. For PC mutants with the anchoring groups assumed to be 'face down' for covalent binding to gold, one expects a vertical size of about 2.8 nm. Therefore, data for PCSS are centred at a value close to that expected, whereas the vertical dimension of PCSH above the gold substrate slightly differs from this value. The standard deviation, which is in both cases much larger than the experimental error, is indicative of a significant spread in the vertical size of the molecule. This result suggests that the disulfide bridge provides a stricter immobilisation and a more homogeneous orientation of PCSS molecules onto gold compared to PCSH, where the single thiol, external to the main structure, could allow a higher flexibility of the adsorbed proteins.

The adsorbed PCSS and PCSH molecules have been also imaged by STM in buffer solution, air and under nitrogen atmosphere. No substantial differences in shape between the two mutants could be observed in the correspondent STM images. For both PC mutants, the STM images appear to be stable and reproducible even after repetitive scans, thus confirming a robust binding of the protein molecules to Au(111) substrate. Some representative STM images are shown in Fig. 4 for PCSS on Au(111) under various experimental conditions

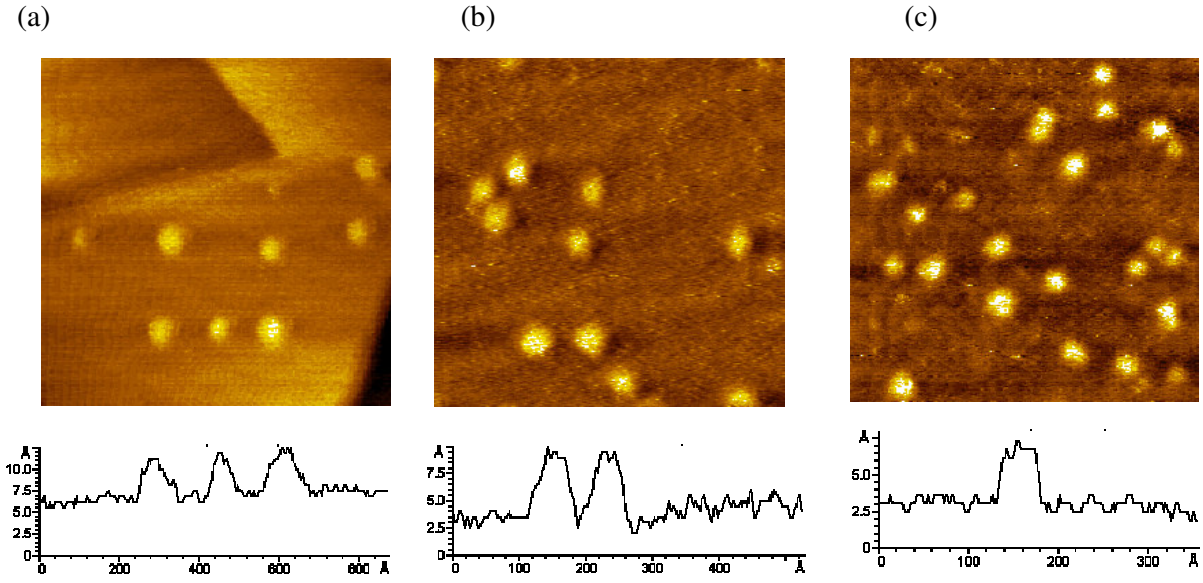

Fig. 4: STM images of PCSS molecules on Au(111) recorded in aqueous medium (a), in air (b), and in nitrogen atmosphere (c).

The lateral dimension of these single molecules well agrees with the crystallographic values of PCSS showing a diameter of about 4.0 nm. The vertical size of PCSS and PCSH is ranging between

0.5-0.7 nm, as measured by the tip retraction along the z axis and shown in the cross section profile of Fig. 4. The vertical size appears to be underestimated and significantly smaller than that expected, as generally observed for the biomolecules imaged by STM. This recurrent characteristic of the STM images from biological material has drawn our attention, especially regarding the possibility that the tip may interfere with the soft biological sample during the imaging scans.

We have, therefore, estimated the tunnelling gap between the scanning tip and the gold substrate as deeply discussed in **ref. 13**. Briefly, the tip-sample separation can be inferred from the tunnelling current and bias voltage settings, once the corresponding tunnelling resistance has been calibrated against the gap width. In Fig. 5 the dependence of the resistance on the tip-substrate distance is shown, in air and in water, on an Au(111) substrate by using a Pt-Ir tip. Here, the initial tip position (Z = 0 nm) refers to a tunnelling resistance of 4 x 10^9 Ω, while maximum tip extension corresponds to a contact resistance of 2 x 10^4 Ω. From data in Fig. 5 we inferred tunnelling distances of about 3 nm and 6 nm in water and in air, respectively, at a working resistance of 4 x 10^9 Ω.

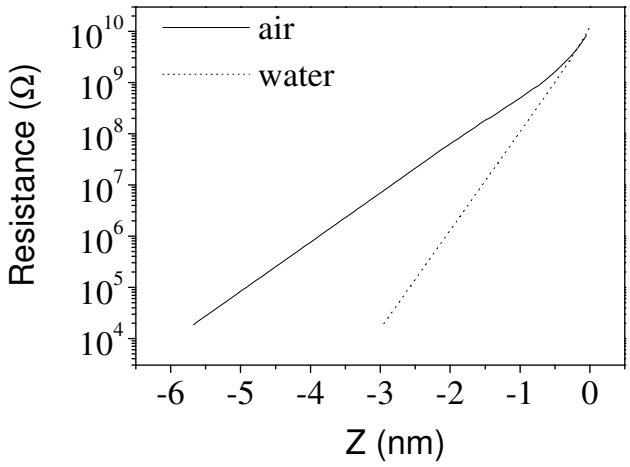

Fig. 5: Tunnelling resistance measured on a flat Au(111) substrate and plotted, in semi logarithmic scale, against the vertical tip position (distance spanned by the tip).

During the last year, we have also focused on the relevance of tunnelling distances when imaging soft biological material, specifically PC mutants chemisorbed on Au(111) **(ref. 13).** A clear evidence of the possible tip-molecule interaction, once the tunnelling distance is reduced, is shown in the sequence of STM images as recorded in water for PCSS (Fig. 6). As inferred by the resistance-distance plot of Fig. 5, the tunnelling gap width was initially reduced from 2.9 nm (Fig. 6 (a)) to 2.4 nm (Fig. 6 (b)). If a tip retraction of 0.5 nm is added to such distances, in both cases the tip has enough vertical space to overcome the proteins, without interfering with their molecular structure. In full accordance, no changes in shape or lateral dimensions were observed for the imaged proteins.

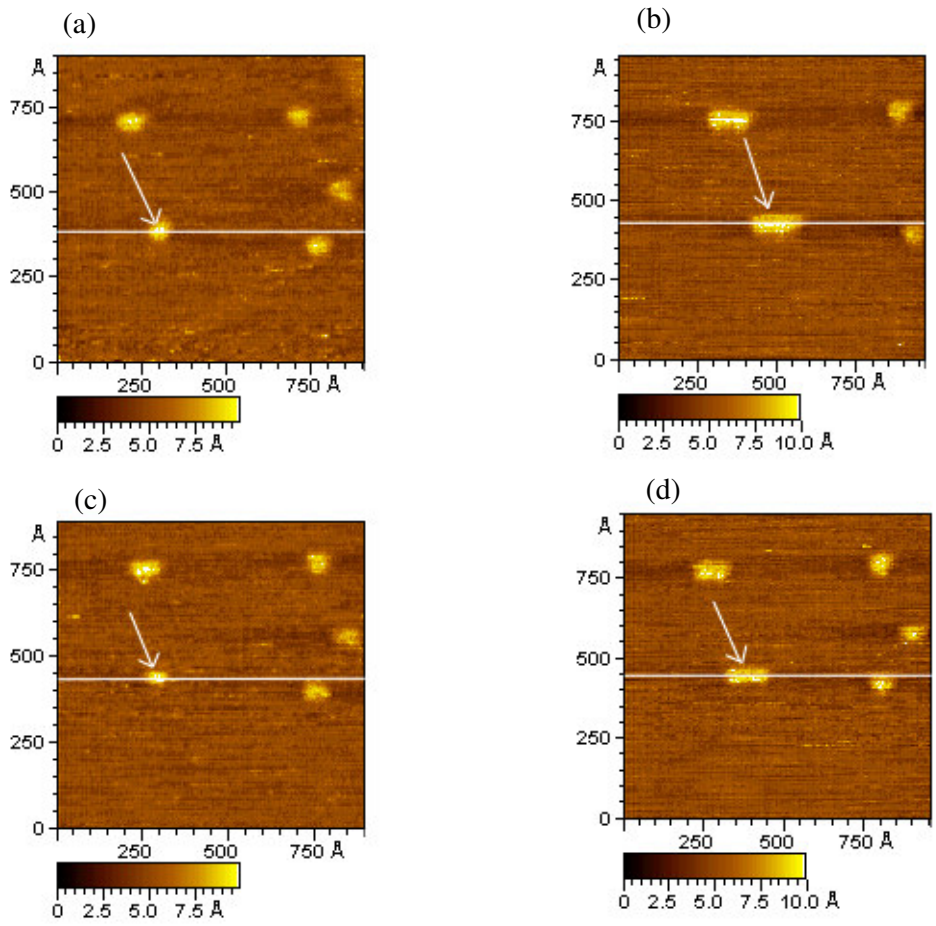

Fig. 6: PCSS proteins adsorbed on an Au(111) substrate as imaged by constant current STM in ultra pure water at decreasing tunnelling resistances: 4 x 10^9 Ω (a), 4 x 10^8 Ω (b), 4 x 10^7 Ω (c), 2 x 10^7 Ω (d).

On the contrary, when the tunnelling gap was reduced to 1.9 nm (Fig. 6 (c)) by setting the resistance to 4 x 10^8 Ω, the available vertical space results to be 2.5 nm, which is below the physical height of the proteins. As a major consequence, some PCSS molecules display a considerable enlarged lateral dimension. For example, the molecule indicated by the white arrow increases its lateral size from 5.7 nm (Figs. 6 (a), (b)) to 14.9 nm (Fig.6 (c)). Finally, when the resistance is set to 2 x 10^7 Ω (Fig. 6 (d)), which corresponds to a tip-substrate distance of 1.4 nm, the lateral size of the indicated PCSS molecule is enlarged to a value of 16.9 nm. At the last two tunnelling resistances, the tip can either squeeze or pass through the protein, leading to invasive measurements of the biological sample.

The strong interaction locally applied could affect either the structure or the function of the bio-molecule, preventing any investigation of the intrinsic electron transport properties. Such results

indicate that STM is a powerful technique to image and study single biomolecules if care is taken in setting the resistance values corresponding to non invasive tip-substrate distances.

Functionality and redox activity of adsorbed molecules

The study on the functionality of PC mutants monolayer covalently immobilised on gold electrode was addressed by CV, and performed in a collaboration with the Oxford group **(ref. 11).**

In these measurements robust voltammetric responses, stable to continual scanning (>100 cycles at 10 mVs^{-1}), were obtained for PCSS adlayers on polycrystalline gold as shown in Fig. 7(a). The redox midpoint potential of the PCSS adlayer was 162 ± 10 mV vs SCE, a value close to that obtained diffusively with the wild-type protein at edge oriented pyrolytic graphite electrode. This confirms that immobilization at the gold surface is occurring without significant perturbation of the native structure.

The surface coverage of electroactive molecules, estimated by integrating the faradaic response, and correcting for an AFM-determined surface roughness factor of 1.3, was of 2-8 × 10^{14} molecules/cm^2. This value is in good agreement with an expected coverage for a molecule with a lateral dimension of ~3.5 nm, and indicates that immobilisation occurs with a high degree of functional retention.

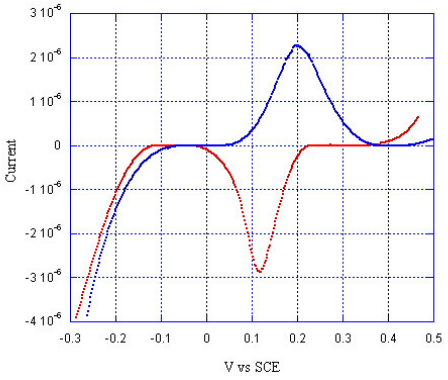

Fig. 7: Background corrected voltammogram recorded for PCSS monolayers in 100 mM potassium phosphate pH 7.14.at 100 mV/s scan rate.

Typical voltammograms recorded on PCSH immobilised on gold are represented in Fig. 8, for increasing scan rates. Independently of the sweeping rate, two well distinct peaks due to the oxidation and reduction process are evident. The high symmetry of voltammograms and the peak separation, very close to the theoretical value, indicates that the redox process is fully reversible and almost ideal.

To estimate the redox midpoint and the surface coverage, the background current generated by the gold electrode in buffer was subtracted to the cyclic voltammogram recorded on the PCSH adlayers on gold. The redox midpoint for PCSH molecules immobilized on bare gold was found to be +168 mV_{SCE} ± 10 mV, a value close to that obtained diffusively with the wild-type protein and the PCSS mutant. The integration of the faradaic current provided an estimate of the electrode coverage value in excellent agreement with that of a densely packed PCSH layer.

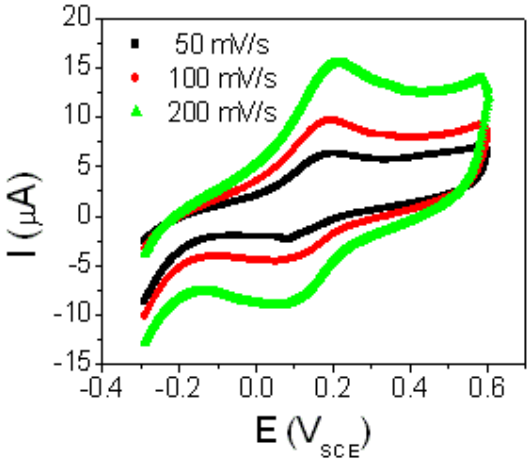

Fig. 8: Voltammograms recorded for PCSH adlayers on bare polycrystalline gold in 20 mM sodium phosphate at pH 6.

Molecular conduction of Plastocyanin mutants

The redox functionality of single PC mutants, as well as the role of the redox centre in the tunnelling mechanism, has been investigated by STM under electrochemical control **(ref. 7)**.

Briefly, in situ STM images for PCSS and PCSH adsorbed on Au(111) for several substrate potentials have been obtained. The molecular features are clearly visible for substrate potentials close to the midpoint potential, the image contrast is weaker when the potential is far from this value and it is recovered once the initial potential is re-established. Such findings seem to be consistent with results reported elsewhere for AZ **(ref. 3)** and to support that copper site represents a preferential way for the tunnelling process through a redox molecule, once its redox levels are properly aligned with the substrate and tip Fermi levels. On the other hand when similar STM experiments have been performed for the PCSH mutant no variation in the image contrast was detected. Since the redox functionality of adsorbed mutant was demonstrated in the corresponding CV experiments, it was hypothesized that the higher protein flexibility resulting from immobilisation via external SH group may lead to an unfavourable alignment of molecular redox levels with tip and substrate Fermi levels.

The stable binding of the PC mutants allowed studying the conductive behaviour of individual molecules by Scanning Tunnelling Spectroscopy, which was initially carried out in ambient condition **(refs. 7, 12)**. For both PCSS and PCSH, current-voltage measurements were recorded by positioning the tip over individual molecules after having disengaged the feedback loop.

I-V data in the ± 1 V range were compared with those obtained on Au(111) substrates (Fig. 9). The slight asymmetry observed for gold finds an explanation in the atomic structure of the tip apex, which has been theoretically and experimentally demonstrated to influence the I-V relation. PCSS molecules exhibit a reproducible and significant asymmetry when compared to gold. In contrast, only a slight asymmetric I-V relation for PCSH is observed, being however almost indistinguishable from that of gold within the experimental error **(ref. 12)**.

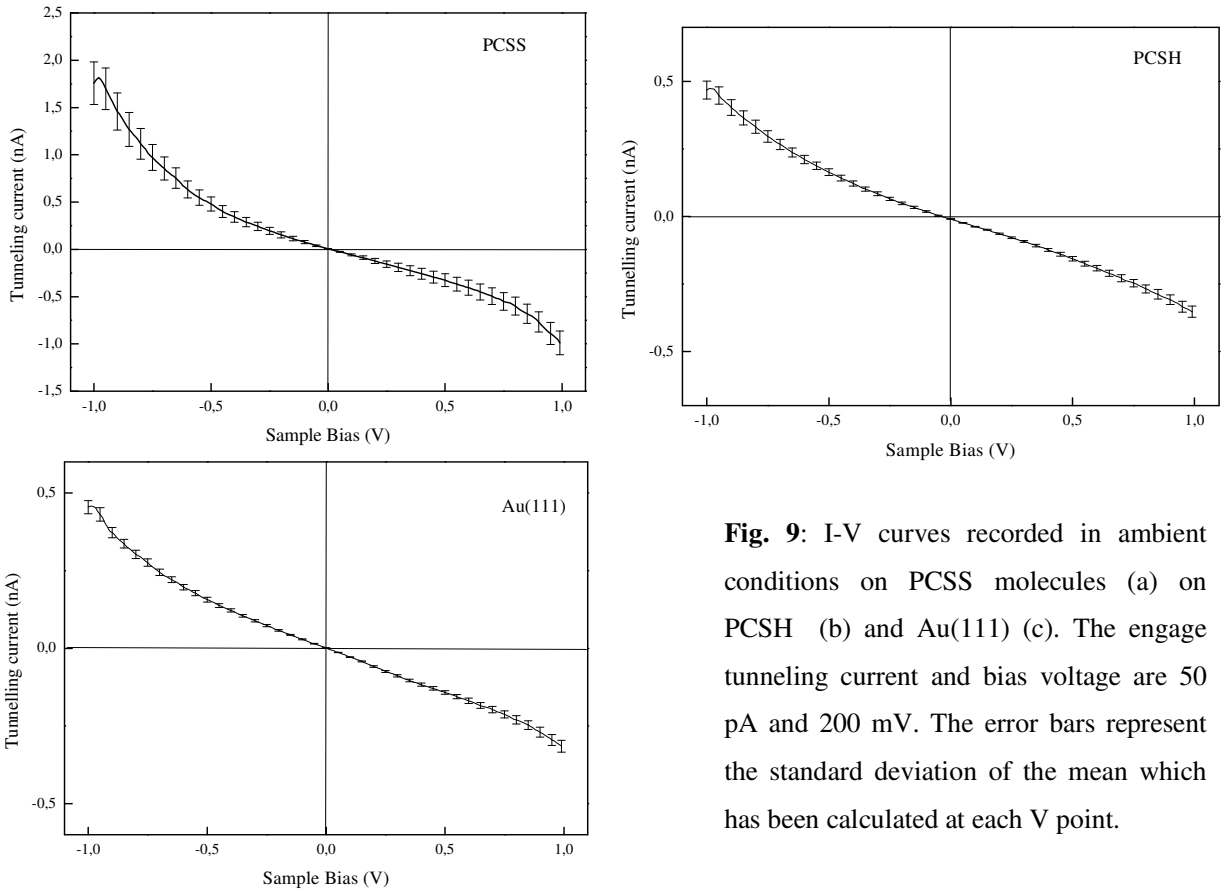

Fig. 9: I-V curves recorded in ambient conditions on PCSS molecules (a) on PCSH (b) and Au(111) (c). The engage tunneling current and bias voltage are 50 pA and 200 mV. The error bars represent the standard deviation of the mean which has been calculated at each V point.

Although both mutants seem to be electronically coupled to the electrode, the origin of the observed differences is presently not clear.

In this connection, more recently, we have revisited the conduction properties of PCSS and PCSH by STS and Conductive AFM (CAFM) in controlled environment **(refs. 12, 14)**.

STS analysis was performed under nitrogen atmosphere, to reduce the water layer at the sample interface which may play a relevant role in tunnelling mechanism **(ref. 12)**. Fig. 10 shows that for both pure gold substrate and PCSH on gold, I-V curves closely resemble those obtained under ambient conditions, whereas the asymmetry observed for PCSS molecules has almost disappeared, with a concomitant decrease of the recorded current.

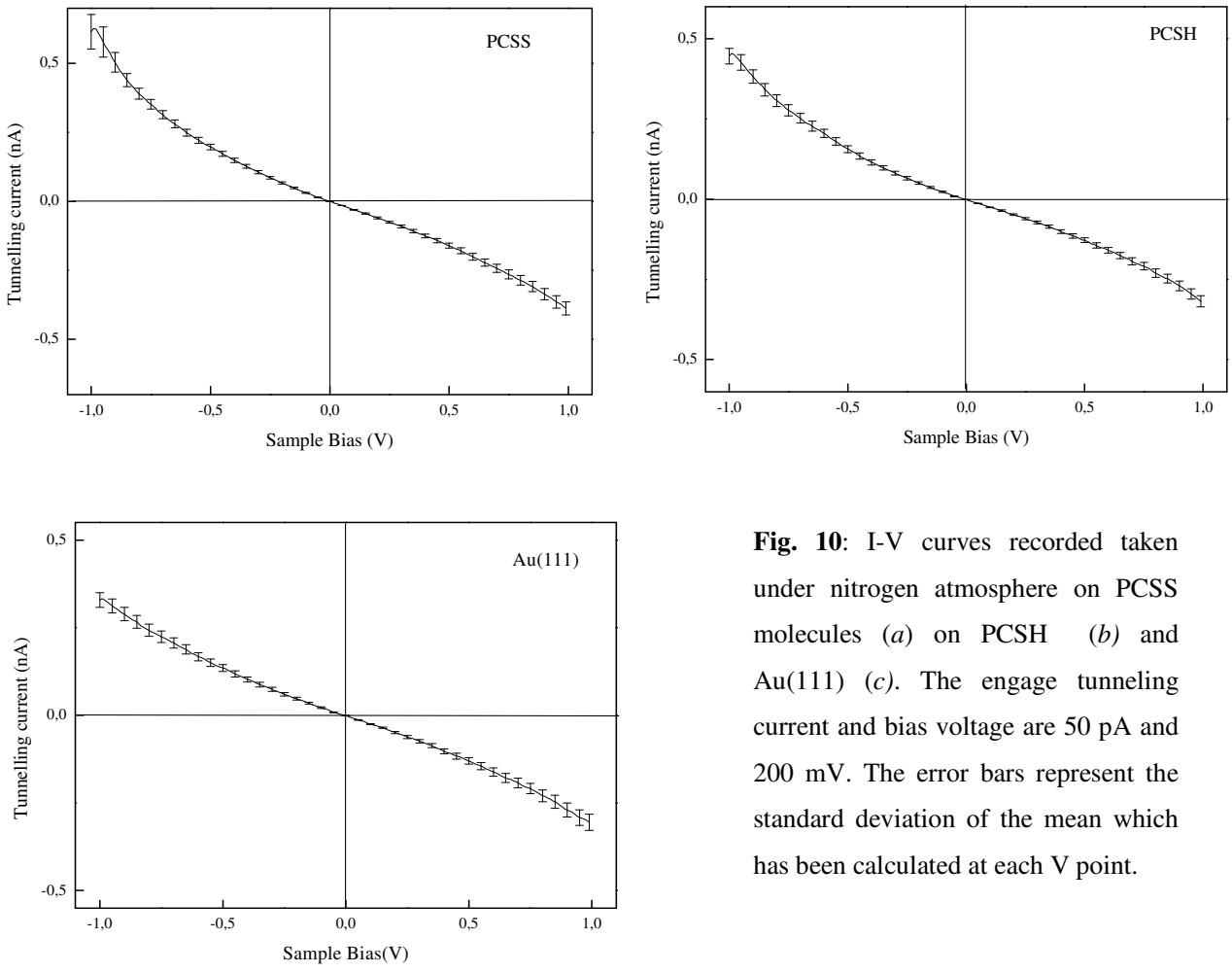

Fig. 10: I-V curves recorded taken under nitrogen atmosphere on PCSS molecules (*a*) on PCSH (*b)* and Au(111) (*c)*. The engage tunneling current and bias voltage are 50 pA and 200 mV. The error bars represent the standard deviation of the mean which has been calculated at each V point.

It can be reasonably assumed, therefore, that water molecules adsorbed at the sample-tip interface are involved in generating the observed PCSS asymmetry. Nevertheless, it appears intriguing that PCSH presents a symmetric I-V relation under both experimental conditions. Indeed, it is hard to conceive that PCSH would retain a different level of humidity with respect to the PCSS mutant.

We might perhaps invoke some differences between the orientation and interfacing of the two mutant proteins with the electrode surface. In the case of PCSH, binding to gold through the thiol group at the carboxy-terminal free end might lead to a less hindered protein surface-electrode coupling than that obtained via the S-S bridge.

In order to investigate the influence of the tip-molecule gap on STS spectra, I-V characteristics of tunnelling junctions, for different values of initial tunnelling current were further measured (**ref. 15**). I-V plots recorded at fixed location on PCSS molecules by varying the initial tunnelling current are shown in Fig. 11. I-V response is asymmetric at all the engaging tunnelling current values examined, even though the amount of rectification decreases as the tunnelling current is raised. These data support a notable dependence of conductive properties on tunnelling gap width.

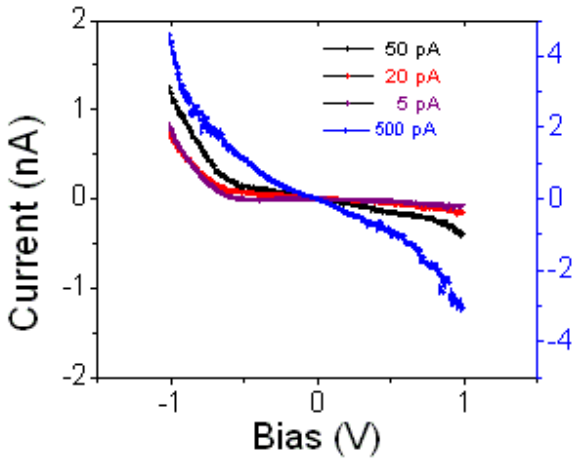

Fig. 11. I-V characteristics recorded by STS on a monolayer of PCSS on Au(111) in ambient conditions. Each curve was recorded at a different initial tunnelling current.

We also expanded the voltage range to study the effect of the applied bias on the electrical response. A sequence of I-V curves was recorded at the same location by extending the bias range to ± 3 V (Fig. 12). An abrupt change was observed when applying ± 3 V with a corresponding unusual increase in current flowing. Nevertheless, the initial conductivity was recovered as soon as the bias range was reduced below ± 2 V. This last finding indicates that at high voltages the bio-molecule was not damaged, but only subjected to transient phenomena induced by the strong local electric field applied by the STM tip.

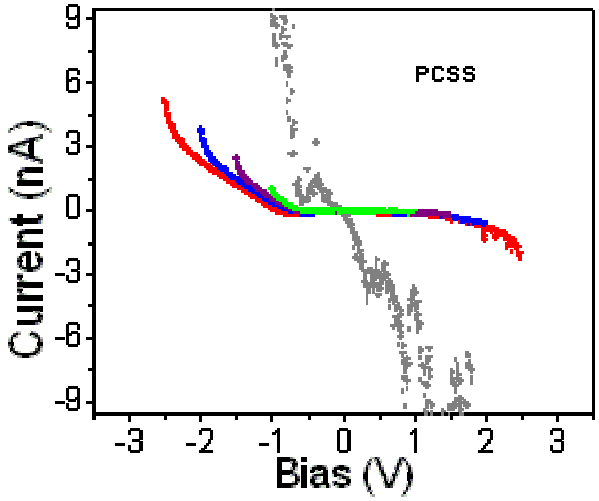

Fig. 12: I-V characteristics recorded by STM on PCSS molecules on Au(111) in ambient conditions, at increasing bias voltage ranges ±1 V (green curve), ±1.5 V (purple curve), ± 2 V (blue curve), ±2.5 V (red curve) and ±3 V (grey curve).

I-V characteristics recorded at 5 and 50 pA on PCSH molecules are shown in Fig. 13. A highly asymmetric I-V response at low starting tunnelling current is observed, as for the PCSS mutant. However, in contrast with what observed with PCSS, the asymmetry completely disappears as the tunnelling gap is lowered.

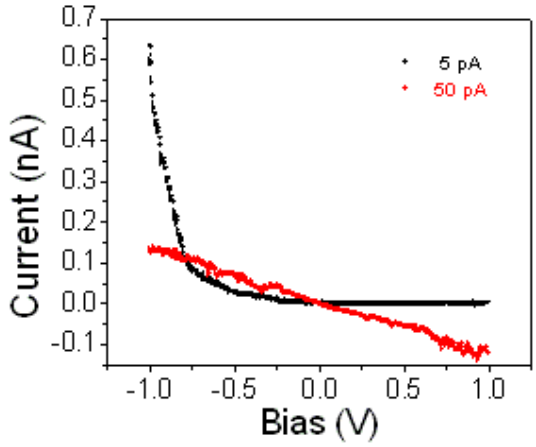

Fig. 13: I-V characteristics as recorded by STS in ambient conditions on PCSH molecules chemisorbed on Au, starting bias 0.2V.

In summary, the STS analysis performed on single molecule pointed out that the protein molecule conduction properties are subtly affected by the water content and are strongly dependent on the tunnelling gap width; with some role played by the particular way in which the proteins assemble on the substrate.

As concerning the tunnelling gap, the conductive properties of plastocyanin mutants have been more controllably investigated by CAFM (**refs. 14, 15**). In this case the AFM tip is positioned in

close contact with the protein molecules allowing also to probe electronic properties of the plastocyanin mutants as a function of the applied forces. The PCSS molecules were either immobilised on gold substrates and contacted with a gold coated tip (Fig.14a) or alternatively adsorbed on gold coated AFM tip which was brought in contact with a flat gold surface (Fig.14b).

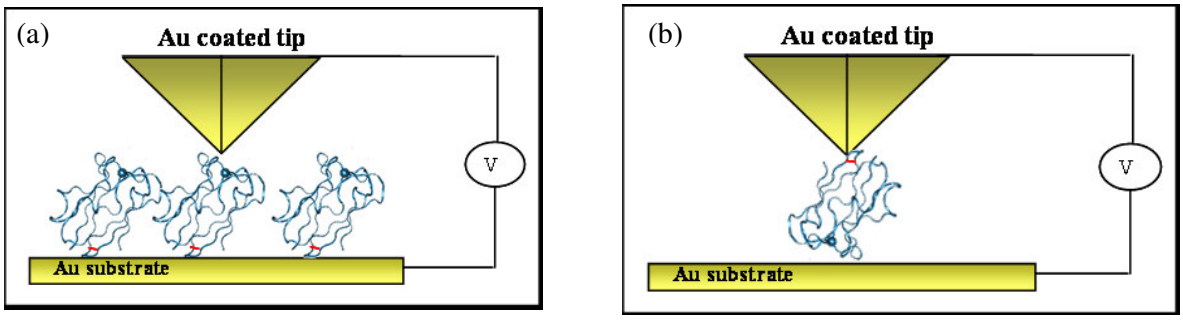

Fig. 14: Schematic representation of tip-PCSS-gold substrate junctions obtained by immobilizing PCSS with the engineered SS group either on gold substrate (a) or on gold coated tip (b). In the first case the junction is formed by bringing the tip into contact with the protein molecules, whereas in the second case the PCSS modified tip is approached to a flat gold surface until a physical contact is established.

I-V characteristics of the PCSS immobilised on gold substrates have been recorded in air at room temperature. For a restricted bias region (± 0.05 V), a pure ohmic I-V relation was found for different applied forces (Fig. 15). At similar forces, as the bias range was increased up to ± 0.3 V, the I-V relation showed a sigmoidal trend (inset of Fig. 15).

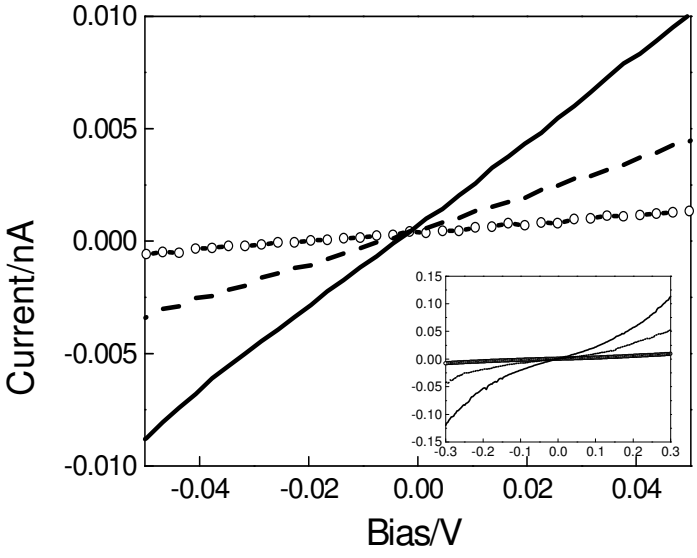

Fig. 15: I-V characteristics over ± 0.05V, measured in ambient condition, for a gold coated AFM tip in contact with PCSS molecules immobilized on Au(111) substrate at applied loads of 2nN (*open circle*), 4nN (*dashed line*), 8nN (*solid line*). Inset shows the sigmoidal I-V relation over ± 0.3V for 2nN (*open circle*), 4nN (*dashed line*), 8nN (*solid line*) .

For a wider bias range (± 3 V), two current peaks were observed at about –1.2 V and +1.8 V (Fig. 16). I-V spectra were quite reproducible when repeated at the same position above the sample. The two peaks seem to be reminiscent of a resonant electron transport, which was already observed for junction including electro-active moieties, and related to an electron transport involving the redox centre. However, we noticed that both peak position and current intensity were found significantly dependent on the tip position. These changes possibly reflect local variation within the junction, in terms of different orientation and/or number of proteins involved.

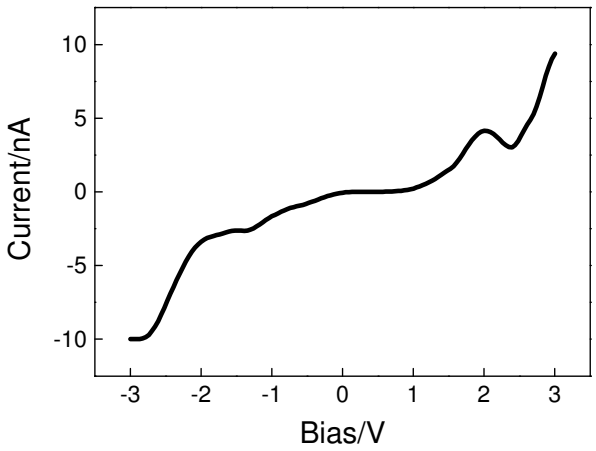

Fig. 16: I-V curves recorded for a gold coated AFM tip in contact with PCSS molecules immobilized on Au(111) substrate. The measurements are carried out at room temperature under ambient condition by sweeping the bias between ± 3V at a force load of 4nN.

Fig. 17 shows that the conductance, as derived from the slope of the linear portion of the I-V curves, increases immediately after the AFM probe has contacted the monolayer and reaches a constant regime within 8-20 s. In addition, the stronger is the applied force the faster is the transient response observed. This effect is attributed to the presence of attractive capillary forces generated by a thin water layer at the protein/tip interface, when experiments are carried out in air.

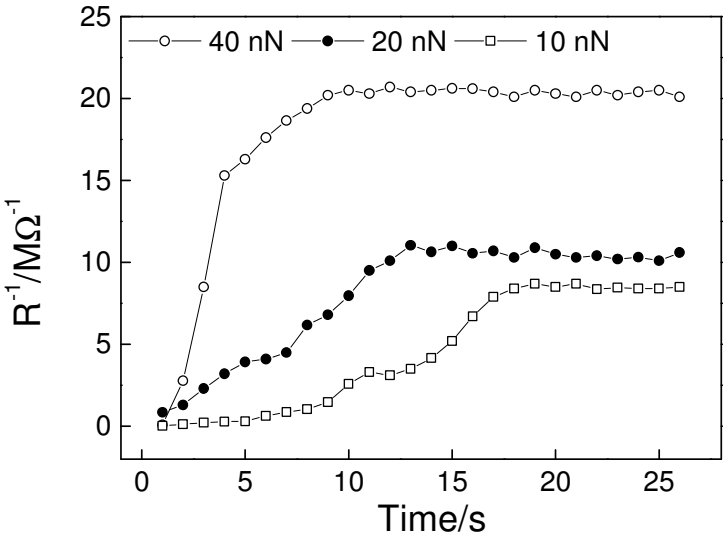

Fig. 17: the conductance, derived from the inverse of the slope for the linear bias region (± 0.05V) of the I-V curve, is plotted versus time for three applied forces (*open circle*), 40nN, (*filled circle*) 20nN, (*open square*) 10 nN.

To minimise the action of capillarity forces, I-V characteristics of PCSS molecules were repeated under nitrogen atmosphere. In these experimental conditions, conductance was observed to remain constant as a function of time (data not shown) and the ohmic region is now extended up to ± 0.3 V (inset Fig. 18). At higher biases (± 1 V) I-V curves present a sigmoidal shape, which is maintained for increasing applied forces as shown in Fig.18. I-V characteristics appear slightly asymmetric, particularly at higher applied forces, as recently seen also for azurin (*Oxford group*). This asymmetry may be due either to the redox active centre asymmetrically positioned within the junction or also to nature of the contacts at the metal-molecule interface. Specifically, in our measurements the protein is chemically coupled to one electrode and physically contacted with the other one.

In Fig. 19, the resistance, as calculated from the 1/slope of the ohmic region, is plotted as function of the applied force. The resistance estimated for PCSS proteins was found to be 10^9-$10^{10}\Omega$ at forces of 3-4 nN. Interestingly, in the corresponding plot two distinct trends are observed. The junction resistance decreases exponentially until 8 nN, whereas for forces higher than 8 nN a more rapid exponential trend is observed. This effect may depend on the nature of the contacts and may be further related to a larger micro contact area achieved with increasing pressure, or to changes in the electronic properties of the deformed protein. Indeed, the discontinuity in the dependence of resistance on applied forces is likely connected to alterations of the three dimensional structure of the protein, which suggests the presence of a critical pressure for PCSS conduction. Generally, the behaviour observed in Fig.19 is reversible when the forces are reduced to the initial values (about 3 nN), thereby indicating that the PCSS molecules are only elastically compressed, and not irreversibly deformed.

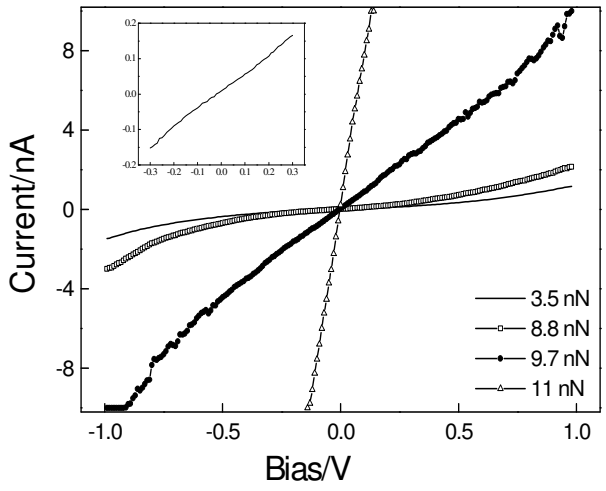

Fig. 18: I-V curves over ±1V, acquired under nitrogen atmosphere, for a gold coated AFM tip in contact with PCSS molecules immobilized on Au(111) substrate at increasing applied forces. Inset shows the linear I-V relation over ± 0.3V.

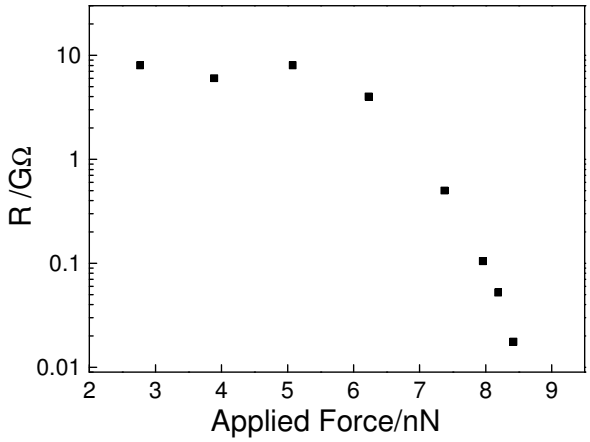

Fig. 19: semilogarithmic plot of junction resistance *vs* increasing compressional forces when the gold AFM tip is brought into contact with PCSS monolayer.

The dependence of the current on contact force was also investigated by recording force-distance curve and current signal at a fixed bias simultaneously. When the measurement is carried out on bare gold, no current flows before the AFM probe has contacted the gold; while at nominal contact (zero distance) the current jumps to values that saturate the pre-amplifier (Fig.20a). With PCSS molecules, as soon as the tip approaches the proteins the current increases almost linearly until a force of about 8 nN (Fig.20b). Then no further increase is recorded up to 20 nN. Above this value the current signal quickly reaches a high value beyond the pre-amplifier limit. These results follow the trend observed in the preceding analysis of junction resistance dependence on contact force, thereby confirming the presence of a critical pressure for PCSS molecules.

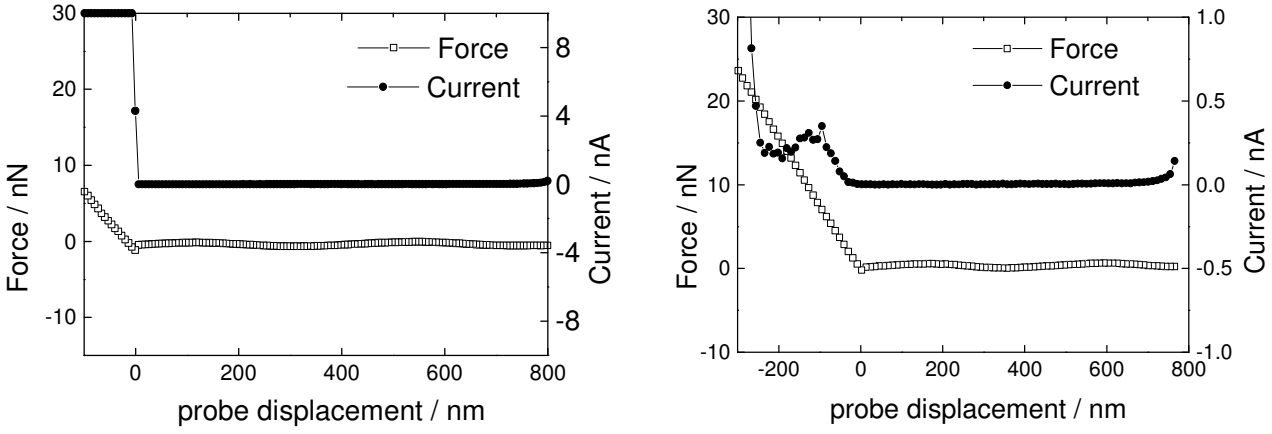

Fig. 20: current/force simultaneously recorded as a conducting AFM cantilever is moved toward the gold surface (a), or toward the PCSS monolayer (b) at a bias of 1V.

The conduction characterisation was repeated for the configuration depicted in Fig. 14 (b), where the bio-molecules were adsorbed on the conductive AFM probe. All major characteristics observed

on the other experimental set-up were reproduced; this indicating that the conduction properties of the metal-PCSS-metal junction, obtained according to the two approaches, are very likely equivalent. Thus, it is reasonable to assume that the distance of the copper site with respect to the gold substrate has no effect on the conduction properties of the biomolecular junction here investigated. The only remarkable difference observed between the two junction geometries regards the dependence of resistance on compressional forces. In fact, the pressure value which determines a discontinuity in the molecular resistance is spread between a few nN and tens of nN. Occasionally, very low applied forces were sufficient to reduce drastically the junction resistance, where an applied force of 4 nN is enough to lower the resistance of two orders of magnitude. This variability can be due either to a different number of molecules included in the junction or to different tip radius which affects the microcontact area and the specific resistance.

The two well defined trends observed for PCSS resistance seem to be consistent with an electron transport mechanism which depends on structural deformations of the compressed protein inside the junction.

The effect of compressibility on conductance was explored on PCSH monolayer as well. The biomolecular junction was formed by contacting PCSH monecules tethered on Au(111) substrates with gold coated AFM probes **(ref. 15).**

Typical I-V characteristics as recorded at different pressures are shown in Fig. 21. All plots appear to be highly symmetric and sigmoidal in shape. The high level of symmetry in the current signal as function of the bias is in agreement with what observed by STS on single molecules of PCSH under controlled atmosphere **(ref. 12).**

Independently of the applied pressure, I-V plots show an ohmic region within ± 0.1 V. This is a quite restricted region as compared with that of PCSS, whose I-V linear dependence was observed up to ± 0.3 V.

The resistance of the protein has been studied also as a function of the force exercised by the conducting AFM probe. Fig. 22 shows that over a range of 15 nN, resistance of the bio-molecular junction decreases upon increasing the force. Even for this PC mutant, the resistance is scaling with two distinct exponential laws. As seen for PCSS, the presence of such discontinuity in the resistance–force dependence confirms the occurrence of an electron transport mechanism dependent on structural deformations of the compressed proteins inside the junction **(refs. 14, 15).**

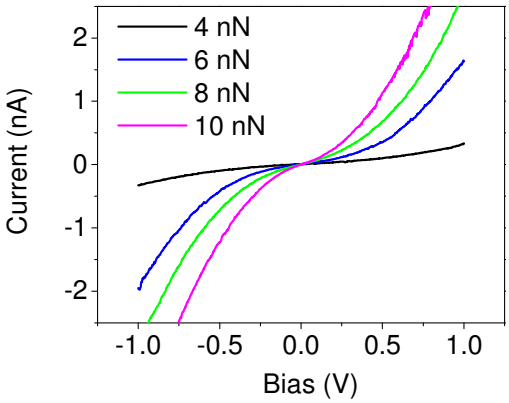

Fig. 21: I-V characteristics as recorded by CAFM on PCSH molecules chemisorbed on Au(111) under nitrogen atmosphere.

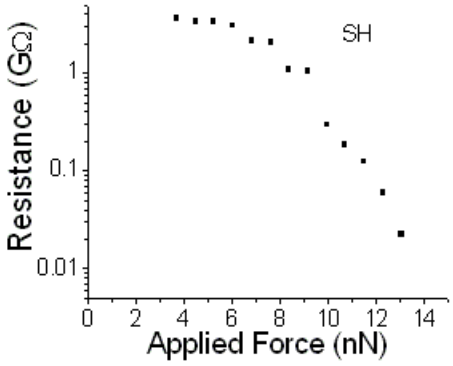

Fig. 22: Semi logarithmic plot of resistance *vs* applied forces obtained by CAFM on a PCSH monolayer under nitrogen atmosphere.

2. Optical Spectroscopy

Pump-Probe

The electron transfer process depends on several parameters which sometimes are difficult to estimate; one of which being the reorganisation energy λ of the nuclear degree of freedom. Calculation of this energy requires a knowledge of the coupling strength of the protein vibrations to the electron transfer event. To get some insight on such a parameter we have previously performed femtosecond laser pump-probe experiments on azurin **(ref. 4)**. More recently, we have extended such a study to copper protein plastocyanin **(ref. 10).**

Due to its wide spectral content, a femtosecond pump pulse creates a population in the excited electronic state and vibrational coherence in both the ground and excited states. A delayed probe pulse interrogates the sample and additional information (with respect to traditional Raman) can be obtained. The evolution of the signal is therefore modulated by the dynamics of the vibrational states. Suitable processing of this signal allows one to extract the dynamics and the vibrational feature of the ground and the excited states of the protein active site.

The results obtained for plastocyanin indicate that the excited state, involved in the charge transfer, decays in a non radiative fashion within about 300 fs (Fig.23).

The vibrational coherence modulating such a decay, when analysed in the frequency domain, reveals all the frequency modes of the conventional Resonance Raman signal (Fig.24).Additionally, some low frequency modes, of collective character and probably of some biological relevance (**refs**

4, 10), are observed in these spectra. Moreover a 500 cm^{-1} mode, not present in the conventional Resonance Raman spectrum and already observed in other copper proteins, appears. An analysis in the time domain indicated that, very likely, it belongs to the vibrational manifold of the excited state.

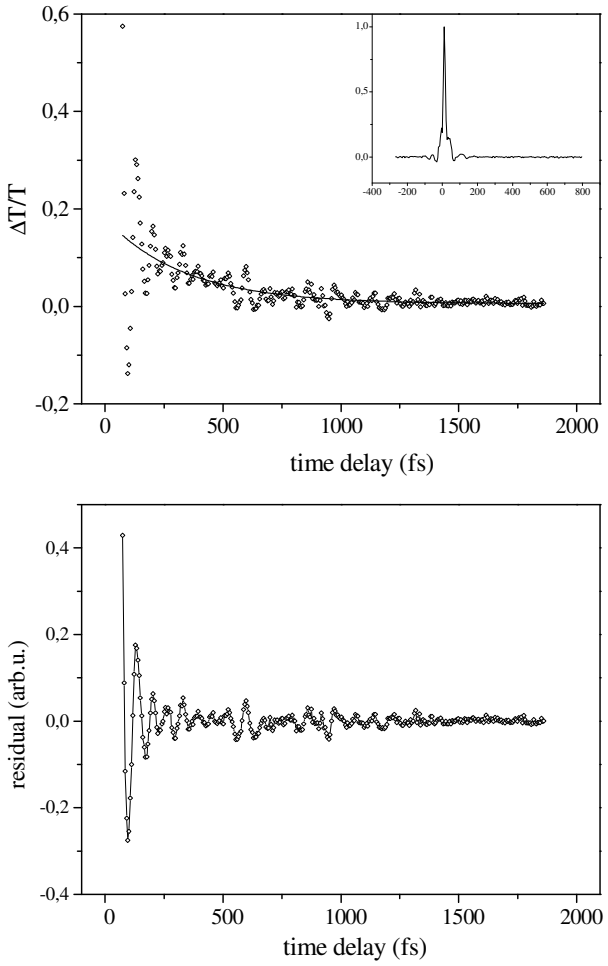

Fig. 23: *Top*: differential optical transmission of PC. The solid line is the best fit of experimental data obtained with a function $y(t) = A + B \cdot e^{-t/\tau}$. Inset: wavelength-resolved pump-probe signal of buffer solution containing no protein. *Bottom*: oscillatory component (residual) obtained after subtraction of the exponential fit from experimental data of the upper plot.

Fig. 24: Fourier spectrum of the residual shown in Fig. 23 bottom.

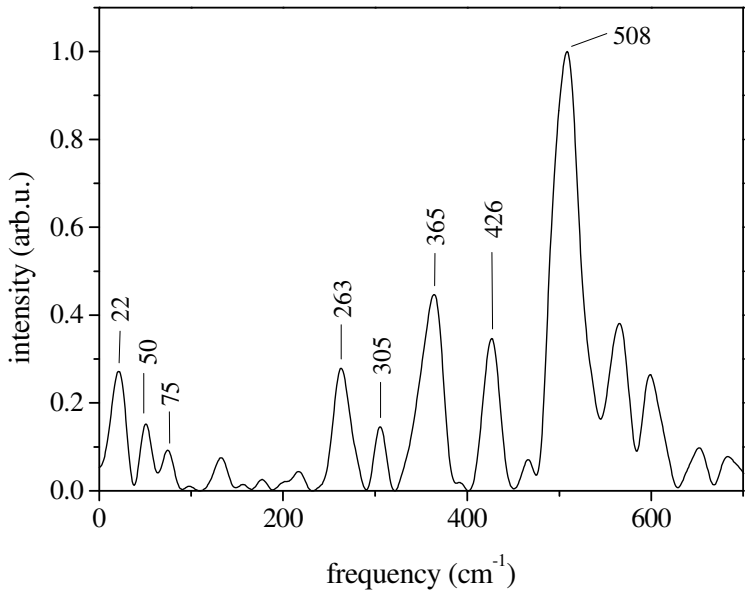

In order to confirm such findings an MDS study of the excited state of plastocyanin was carried out (**ref 10**). According to **ref. 2**, MDS of hydrated plastocyanin has been performed by using the CHARMM package with Charmm27 as force field including TIP3 model for water. By such approach the main Resonance Raman experimental features around 400 cm^{-1} have been reproduced by calculating the Fourier transform of the Cu-S(Cys84) distance autocorrelation functions.

Similarly, the excited state of the copper active site was modelled by increasing the equilibrium bond length in the harmonic Cu-S(Cys84) interaction and by varying the force constant of the same bond. According to this procedure the power spectrum obtained is shown in Fig. 25. A main peak at 511 cm^{-1} appears, thus representing a vibration mode of the excited state of plastocyanin. The fairly good agreement between the MDS and the experimental results gives on one hand support to the experimental findings and, on the other, strengthens the role of MDS in modelling the electron transfer properties of copper proteins.

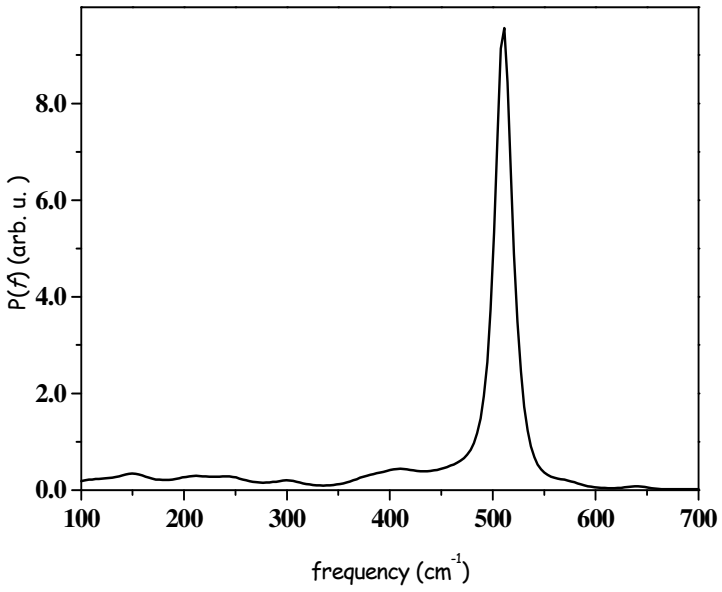

Fig. 25: Power spectrum, as function of frequency, of the Cu-S(Cys84) bond distance fluctuation analysed for 800 ps (see **ref. 10** for details).

3. Molecular Dynamics simulations

In order to get additional information on the self-assembling of plastocyanin mutants on gold substrate, we have conjugated our nanoscopic experiments with MDS studies **(refs. 8, 9, 15)**. In our

model, the interaction between the protein and the gold substrate involves one or two sulfur atoms from the biomolecule, each interacting with three Au atoms. We run a 10 ns-long MDS of plastocyanin mutants by using a Charmm force field for the protein atoms, an TIP3P for hydration water (one layer of water molecule as shown in Fig. 26) **(refs. 8, 9)**.

The root mean square fluctuations (RMSF $<\Delta r^2>^{1/2}$) of both plastocyanin anchored with a single sulfur atom (PCSS-I) ($<\Delta r^2>^{1/2}$=(0.013± 0.005)nm) and with two sulfur atoms (PCSS-II) ($<\Delta r^2>^{1/2}$=(0.015± 0.005)nm) are significantly lower in comparison to that of non immobilised PCSS ($<\Delta r^2>^{1/2}$=(0.03± 0.01)nm). Accordingly, the flexibility of the macromolecule appears affected by the immobilization onto the substrate. The observation that larger RMSF values are revealed in PCSS-II with respect to PCSS-I suggests that the presence of two covalent bonds might yield a larger flexibility at least in same regions of the macromolecule.

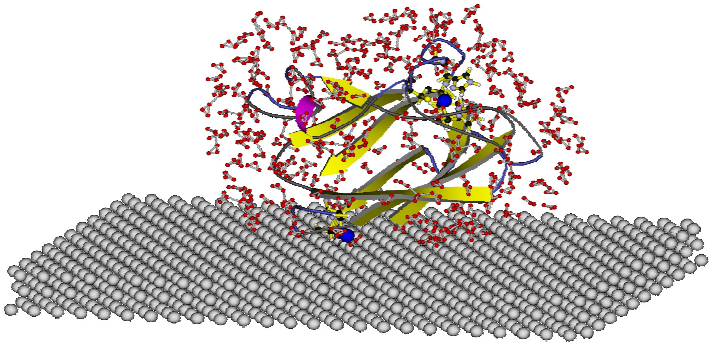

Fig. 26: Plastocyanin mutant immobilised on gold surrounded by a layer of water molecules.

The trend with time of θ and Φ (namely the angles describing the orientation and the precession, respectively, of the protein p axis with respect to gold surface normal), calculated during the MD trajectory, are plotted, for both PCSS-I and PCSS-II, in Fig. 27. In both cases, a significant deviation of **p** from the normal axis is registered. This means that both the gold-anchored systems can assume different orientations with respect to the gold electrode. In addition, the mean value of θ is smaller for PCSS-I than for PCSS-II (see legend of Fig. 27); this means that the protein anchored by a single bond assumes a configuration closer to the normal. Such behaviour might be indicative of a less extensive contact, for PCSS-I, between the protein and the gold atoms.

Furthermore, we note that θ exhibits a larger standard deviation for PCSS-I with respect to PCSS-II (see legend of Fig. 27); such a behaviour being in agreement with a higher degree of freedom for

PCSS-I with respect to PCSS-II. Concerning Φ, PCSS-I and PCSS-II show different average values, reflecting a different average position of the macromolecule with respect to the gold substrate. Interestingly, a much larger standard deviation of Φ is observed for the PCSS-I in comparison with PCSS-II (see legend of Fig. 27).

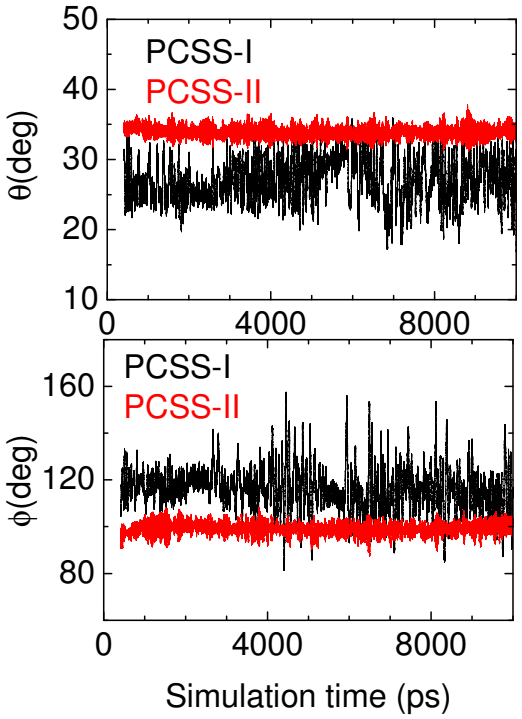

Fig. 27: Temporal evolution, along a 10 ns MD trajectory, of θ and Φ angles describing the orientation and the precession, respectively, of the protein **p** axis with respect to gold surface normal, for the PCSS-I (black) and PCSS-II (red). The mean value and the standard deviation of θ are (27± 3)° and (34± 1)° for PCSS-I and PCSS-II, respectively. The mean value and the standard deviation of Φ are (116± 10)° and (99± 3)° for PCSS-I and PCSS-II, respectively.

Such a result, together with what observed for θ, is indicative that the macromolecule, during its dynamical evolution, can assume different arrangements with respect to the gold surface; such a variability being more marked in the case of a single anchoring point. Notably, the trend of Φ for PCSS-I shows, over the fluctuations, oscillations whose presence points out a sort of periodicity in the lateral movements of the macromolecule anchored by a single sulfur-gold bond.

To compare MDS and AFM data, the protein anchored on gold was described by an ellipsoid centred at the centre of protein mass and oriented according to its main inertial axes (Fig 28). The ellipsoid and its corresponding height over the gold substrate, extracted from the MDS trajectories, are shown in Fig. 29 by sampling structures every 10 ps. It comes out that a single mode distribution is registered for both PCSS-I and PCSS-II. The mean values are, in both cases, close to that expected for the crystallographic data by assuming that protein is anchored to gold via the disulfide bridge (h ~ 3 nm).

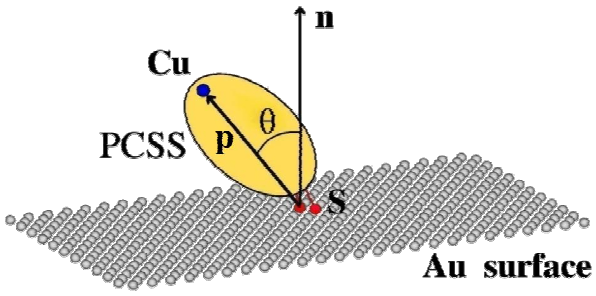

Fig. 28: Scheme of plastocyanin orientation with the respect to the gold surface.

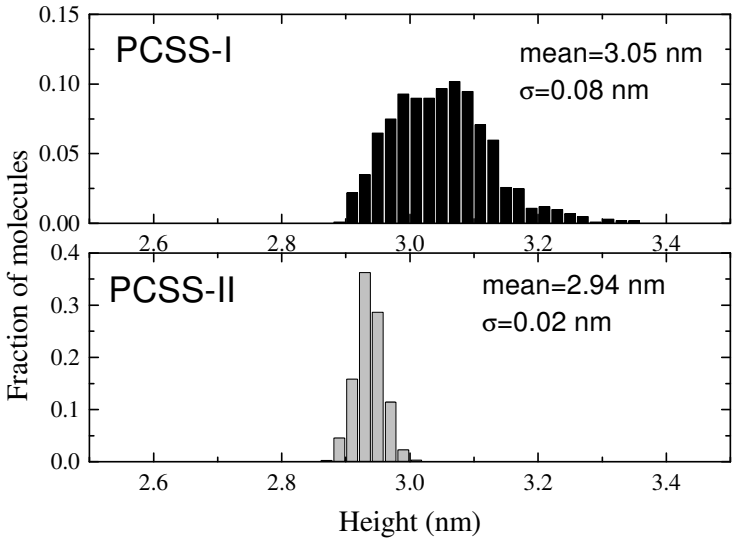

Fig. 29: Statistical analysis of the molecular height above the Au(111) substrate, as extracted from the MDS trajectories for PCSS-I and PCSS-II. The vertical dimension of proteins has been estimated from 1000 molecules sampled every 10 ps of the MDS trajectory.

On the other hand, PCSS-I is characterized by a mean value slightly higher than that of PCSS-II (see the mean values in Fig. 29). Such a finding is consistent with the previous results showing that the protein anchored by a single bond can assume an average configuration closer to the normal to the surface.

For both systems, a spread of heights is registered (see the standard deviations in Fig. 29). Generally, this means that, during its dynamical evolution, the macromolecule, by exploring its accessible conformations, can assume a variety of arrangements, and then of heights, with respect to the gold substrate. On the other hand, we note that PCSS-I is characterized by a wider distribution in comparison with PCSS-II. As a consequence, molecules covalently bound to gold through a sulfur atom show slightly higher flexibility than molecules anchored via two covalent bonds.

These results are in a qualitative agreement with those derived by TMAFM. However, we note that the height distributions, as extracted by MDS, result markedly narrower if compared to those derived by TMAFM. To explain such discrepancies, different effects should be taken into account. First, we remark that TMAFM data refer to a collection of molecules, likely in different starting arrangements, which, moreover, may be anchored to gold by one or both sulfur atoms, whereas MDS considers only a single molecule and the two different ways of anchoring separately. Additionally, it should be taken into account that a further contribution to the structural and dynamical heterogeneity of the adsorbed protein could arise from the complex interaction between the protein and the gold surface. A more accurate modelling of this interaction should be introduced in the MDS. Finally, it should be stressed that TMAFM is sensitive to protein movements on a much longer time scale (at least milliseconds if we refer to a tapping frequency in the range of kHz). Therefore, it can be hypothesized that the flexibility of the molecules, on this temporal scale, above the substrate can also contribute to the broadening of the experimental height distribution; during the measurements the proteins assuming different arrangements. Nevertheless, we remark that, even in the restricted temporal window as explored by MDS, our data show that the proteins can assume a variety of orientations with respect to the gold substrate.

Bibliography

1. M. Milani, L. Andolfi, S. Cannistraro, M. Ph. Verbeet, M. Bolognesi, Acta Cryst. D57 (2001) 1735.
2. A.R. Bizzarri, S. Cannistraro, Chem.Phys.Lett. 349 (2001) 503.
3. P. Facci, D. Alliata, S. Cannistraro, Ultramicroscopy 89 (2001) 291.
4. T. Cimei, A.R. Bizzarri, S. Cannistraro, G. Cerullo, S. De Silvestri, Chem.Phys.Lett. 362 (2002) 497.
5. L. Andolfi, S. Cannistraro, G.W. Canters, P. Facci, A.G. Ficca, I.M.C. Van Amsterdam and M.Ph. Verbeet, Arch. Biochem. Biophys. 399 (2002) 81.
6. A.R. Bizzarri, S. Cannistraro, Appl. Spectrosc. 56 (2002) 1531.
7. L.Andolfi, B.Bonanni, G.W.Canters, M.Ph. Verbeet, S. Cannistraro, Surface Science 530 (2003) 181.
8. A.R. Bizzarri, B. Bonanni, G. Costantini, S. Cannistraro, Chem.Phys.Chem. 4 (2003) 1189-1195.
9. A.R. Bizzarri, G. Costantini, S. Cannistraro, Biophys.Chem. 4 (2003) 1189-1195.
10. T. Cimei, A.R. Bizzarri, G. Cerullo, S. De Silvestri, S. Cannistraro, Biophys. Chem. 106 (2003) 221-231.
11. L. Andolfi, D. Bruce, S. Cannistraro, G.W. Canters, J.J. Davis, H.A.O. Hill, J. Crozier, M. Ph. Verbeet, C.W. Wrathmell, Y. Astier, J. Electroanal. Chem. 565 (2004) 21-28.
12. L. Andolfi, G.W. Canters, M.Ph. Verbeet, S. Cannistraro, Biophys. Chem. 107 (2004) 107-116.
13. D. Alliata, L. Andolfi, S. Cannistraro, Ultramicroscopy (2004) in press.
14. L. Andolfi, D.Alliata, S. Cannistraro, Chem. Phys. Chem. (2004) submitted.
15. B. Bonanni, D. Alliata, L. Andolfi, A. R. Bizzarri, S. Cannistraro, in "Progress in Surface Science Research" Nova Science Publishers, Inc. (2004) in press.